


Article

Spatiotemporal Variation and Driving Factors for NO₂ in Mid-Eastern China

Mingjian Yi ^{1,2} , Yongqing Jiang ^{1,*}, Qiang Zhao ¹, Junxia Qiu ¹ and Yi Li ¹

¹ School of Environment and Energy Engineering, Anhui Jianzhu University, Hefei 230601, China; mjyi@ustc.edu.cn (M.Y.); zhaoqiang@ahjzu.edu.cn (Q.Z.); qjx@stu.ahjzu.edu.cn (J.Q.); ly@stu.ahjzu.edu.cn (Y.L.)

² Anhui Provincial Key Laboratory of Environmental Pollution Control and Resource Reuse, Hefei 230601, China

* Correspondence: jyq@stu.ahjzu.edu.cn; Tel.: +86-139-6598-4929

Abstract: Nitrogen dioxide (NO₂) is one of the major air pollutants in cities across mid-eastern China. Comprehending the spatial and temporal dynamics of NO₂ drivers in various urban areas is imperative for tailoring effective air control strategies. Using data from ground-based monitoring stations, we investigated the impact of socioeconomic and meteorological factors on NO₂ concentrations in cities in mid-eastern China from 2015 to 2021 using the Geographically and Temporally Weighted Regression (GTWR) model. The findings reveal a notable reduction of over 10% in NO₂ concentrations since 2015 in most cities, notably a 50.5% decrease in Bozhou. However, certain areas within Anhui and Jiangsu have experienced an increase in NO₂ concentrations. Significant spatial heterogeneity is observed in the relationship between NO₂ concentrations and influencing factors. The permanent population density (POP) and the electricity consumption (EC) of the entire society exhibited the strongest correlations with NO₂ concentrations, with average coefficients of 0.431 and 0.520, respectively. Furthermore, other economic factors such as urbanization rate (UR), the share of secondary sector output in total GDP (IS), and the coverage rate of urban green areas (CG) were predominantly positively correlated, while GDP per capita (PGDP) and civil car vehicles (CV) demonstrated primarily negative correlations. Furthermore, we examined the correlations between four meteorological factors (temperature, relative humidity, wind speed, and precipitation) and NO₂ concentrations. All these factors exhibited negative correlations with NO₂ concentrations. Among them, temperature exhibited the strongest negative correlation, with a coefficient of −0.411. This research may contribute valuable insights and guidance for developing air emission reduction policies in various cities in mid-eastern China.

Keywords: nitrogen dioxide (NO₂); GTWR; spatial heterogeneity



Citation: Yi, M.; Jiang, Y.; Zhao, Q.; Qiu, J.; Li, Y. Spatiotemporal Variation and Driving Factors for NO₂ in Mid-Eastern China. *Atmosphere* **2023**, *14*, 1369. <https://doi.org/10.3390/atmos14091369>

Academic Editors: Kumar Vikrant, Nikolaos P. Theodossiou, Jibrán Khan, Kostas Karatzas and Eden Mamut

Received: 8 July 2023

Revised: 15 August 2023

Accepted: 28 August 2023

Published: 30 August 2023



Copyright: © 2023 by the authors. Licensee MDPI, Basel, Switzerland. This article is an open access article distributed under the terms and conditions of the Creative Commons Attribution (CC BY) license (<https://creativecommons.org/licenses/by/4.0/>).

1. Introduction

Recent years have witnessed rapid urbanization and industrialization in China, resulting in a significant rise in air pollution and growing concerns regarding climate issues [1]. NO₂, as a major air pollutant, significantly impacts air quality, plays a significant role in the formation of acid rain and photochemical smog, and serves as a precursor to the formation of PM_{2.5} and O₃ [2,3]. In addition, NO₂ exposure can pose a risk to human health by stimulating the respiratory system [4], leading to diseases such as pneumonia and cancer [5] and triggering mental illness and childhood asthma [6,7]. Furthermore, elevated concentrations of NO₂ can negatively impact vegetation growth and harm local ecosystems [8].

The spatial and temporal analysis of NO₂ using satellite data from the Ozone Monitoring Instrument (OMI) of the National Aeronautics and Space Administration has been extensively studied [9]. By analyzing the changes in tropospheric NO₂ vertical column density in East China from 2005 to 2020 to investigate the factors contributing to the reduction in tropospheric NO₂ during the COVID-19 outbreak [10], Zheng et al. [11] analyzed

the long-term distribution characteristics of NO₂ concentrations in the Inner Mongolia urban cluster from 2005 to 2016 revealing an initial upward trend followed by a subsequent downward trend. However, OMI satellite data are often limited by poor resolution and a high number of missing values [12]. Moreover, it does not capture small-scale changes in concentrations [13]. Consequently, studies investigating spatial and temporal variability frequently rely on data obtained from ground-based monitoring sites. For example, recent research conducted by Hůnová et al. [14] documented a significant decrease in NO₂ concentrations at various locations in the Czech Republic. Similarly, Shen et al. [15] observed an increase in the diurnal variation in NO₂ concentrations in eastern China, which was attributed to changes in anthropogenic emissions.

Currently, it is a long-term strategic priority for China's national development to actively promote pollution reduction. Therefore, investigating the relationship between changes in NO₂ concentration and driving factors has emerged as a prominent research topic. NO₂ concentrations typically vary due to three primary factors: emissions, meteorology, and atmospheric chemical processes [16,17]. High temperatures, precipitation, and higher wind speeds have been identified as beneficial factors in reducing NO₂ concentrations [18,19]. Social factors, including industrial emissions, traffic emissions, energy consumption, industrial structure, and population density, have been recognized as essential influencers affecting NO₂ concentrations [20–22]. Wang et al. [23] analyzed the factors driving vehicle NO_x emissions from 2005 to 2015 and identified economic development and road vehicle carrying capacity as the primary drivers of emissions growth. Xu et al. [24] discovered that different levels of urbanization have varying effects on NO_x emissions. Zhang et al. [25] examined NO_x emissions and intensity changes in China and demonstrated that energy efficiency improvements and end-of-pipe emission reduction treatments were effective in reducing NO_x emissions. They found that the main impediment to reducing NO_x emissions and intensity was the final demand effect, with investment and consumption effects being the primary influences. These studies have characterized NO_x emissions in urban environments from different perspectives and identified the main source contributions and potential drivers of NO_x in urban environments. However, we also find that many of these studies have not provided more scientific explanations from the perspective of urban differences or have not paid enough attention to the relationship between urban development trajectories and economic structure as reflected in such differences due to the limited time and space sample size.

Several methods, including structural decomposition analysis [26], index decomposition analysis [27], logistic mean divided index [28], geographical detector model [29], and geographically weighted regression models (GWR) [30], have been employed to study the drivers of NO₂ concentration changes. However, these methods only provide singular insights into NO₂ concentration changes, focusing on a specific time or spatial context. The Geographically and Temporally Weighted Regression (GTWR) model extends the GWR model by constructing a matrix considering spatial and temporal distances. Consequently, it enables a comprehensive reflection of the spatial location characteristics of the model and the influence of temporal factors [31]. The GTWR model has been extensively employed in numerous studies to investigate the spatiotemporal heterogeneity between dependent and independent variables. These studies have examined the impact of population movement on the spread of COVID-19 [32] and identified the primary influences on soil Cd pollution in diverse regions [33], and the spatiotemporal variation in CO₂ emissions resulting from the 'coal-to-gas' conversion in heating areas [34].

In this study, we investigate the trends and spatial characteristics of NO₂ concentrations in central-eastern Chinese cities. The data used for analysis was collected from Chinese air quality monitoring stations between 2015 and 2021. Furthermore, we employ the GTWR model to analyze the spatial and temporal distribution characteristics of the factors influencing changes in NO₂ concentrations. This work aims to understand the trends in nitrogen dioxide concentrations in different cities in the region in recent years and to identify the drivers behind these trends. This may be critical for population health

and environmental protection and provide valuable policy insights and inspiration for the cities involved.

2. Materials and Methods

2.1. Study Areas

The study area encompasses six provincial administrative units in mid-eastern China: Shandong, Henan, Anhui, Jiangsu, Zhejiang, and Shanghai. The topography of each province is as follows: Anhui Province is characterized by plains, hills, and low mountains. The terrain generally exhibits a “high in the south and low in the north” pattern. Zhejiang Province is elevated in the southwest and descends toward the northeast, with mountains and hills being the dominant features. Shandong Province displays a diverse topography, including mountains, hills, and plains. Jiangsu Province is primarily flat and low-lying, mainly comprising plains, while some hilly terrain can be found in the southwest. Henan Province features a mountainous west and a flat east. Shanghai is situated on the front of the Yangtze River Delta Plain, with its terrain being predominantly flat. Figure 1 shows the geographic location of the study area and the distribution of air quality monitoring stations. According to the China Statistical Yearbook in 2022 (<http://www.stats.gov.cn/sj/ndsj/2022/indexch.htm>, accessed on 1 February 2023), the six provincial administrative units within the study area account for 36.89% of China’s GDP and 30.94% of the country’s total population. This region holds great significance in China because it includes the Yangtze River Delta urban agglomeration, which is one of the three largest urban agglomerations in the country. Consequently, the study area has experienced rapid development in recent years, causing advanced industrialization and a substantial influx of people. However, the area’s developed economy, dense population, and high level of industrialization have also contributed to its overall poor air quality.

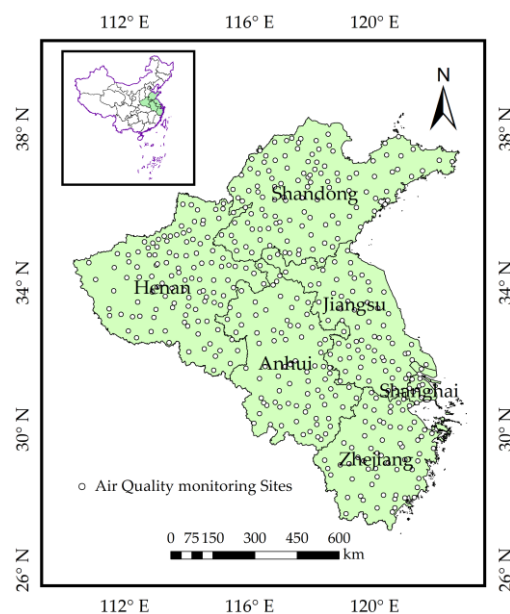


Figure 1. Mid-Eastern China and its monitoring site distribution.

2.2. Data Sources

2.2.1. NO₂ Concentration Data

Hourly NO₂ concentration data for 2015–2021 were obtained from the China General Environmental Monitoring Station (<http://106.37.208.233:20035/>, accessed on 1 February 2023). As of 2023, the country has established over 2000 monitoring stations that measure and record local PM_{2.5}, PM₁₀, SO₂, NO₂, O₃, and CO concentrations on an hourly basis. Every city in the study area has at least one monitoring site, and for cities with multiple monitoring sites, we averaged the corresponding data. Before utilizing the data, any

instances of zero observations were eliminated. To derive daily, monthly, quarterly, and annual concentrations for each city, arithmetic averaging was applied in accordance with the Chinese Ambient Air Quality Standard (GB3095-2012) [35]. This involved ensuring a minimum of 20 hourly average concentrations or sampling times per day, at least 27 daily average concentrations per month, and at least 324 daily average concentrations per year.

2.2.2. Socioeconomic Data and Meteorological Data

Owing to the unavailability of data for county-level cities, this study focuses on collecting socioeconomic data from 74 prefecture-level cities within the study area from 2015 to 2021. The data are obtained from the China Statistical Yearbook and the China Urban Statistical Yearbook, encompassing a range of statistical indicators, including resident population density (POP), GDP per capita (PGDP), urbanization rate (UR), the proportion of secondary industry output to total GDP (IS), social electricity consumption (EC), greening coverage of built-up areas (CG), and civilian car ownership (CV). A total of 4144 data samples were collected, with each indicator sourced from the corresponding year’s statistical yearbook to ensure data consistency across cities. The meteorological data for the period of 2015 to 2021 were acquired from the National Centers for Environmental Information (<https://www.ncei.noaa.gov/>, accessed on 1 February 2023). The data encompass temperature (TEM), precipitation (PRE), relative humidity (RHU), and wind speed (WIN). Daily averages for each meteorological parameter were computed by averaging four observations taken at 02:00, 08:00, 14:00, and 20:00 h, and these values were then aggregated to calculate monthly averages. A comprehensive description of the variables is provided in Table 1.

Table 1. Statistical description of each variable used in the GTWR model.

		Variable	Unit
socioeconomic factors	POP	Permanent population density	10,000 Capita/km ²
	PGDP	GDP per capita	yuan
	UR	Urbanization rate	%
	IS	Share of secondary sector output in total GDP	%
	EC	Electricity consumption of the whole society	kwh
	CG	Coverage rate of urban green areas	%
	CV	Civil car vehicles	car
meteorological factors	TEM	Average temperatures	°C
	RHU	Relative humidity	%
	WIN	Average wind speed	m/s
	PRE	Average precipitation	mm

2.3. Method

2.3.1. k-Means Clustering

Clustering refers to gathering samples with similar characteristics and dividing samples with dissimilar characteristics into categories [36]. Recently, the *k*-means clustering algorithm has gained popularity in data analysis applications due to its ease of implementation, flexibility, and scalability. The *k*-means clustering algorithm utilizes Euclidean distance as a measure of similarity between sample points, where closer sample points indicate a higher degree of similarity. The criterion function for the *k*-means algorithm is the sum of squares error (*SSE*), which measures the density of the sample points, with a smaller *SSE* value indicating a better clustering effect. Let $X = \{x_1, \dots, x_N\}$ denote the set of *N* samples. C_i ($1 \leq i \leq k$) represents a random selection of *K* initial cluster centers. The formulas for the Euclidean distance and the *SSE* are as follows:

$$dis(X, C_i)^2 = \sum_{j=1}^n \|x_j - c_{ij}\|^2$$

$$SSE = \sum_{i=1}^k \sum_{x \in C_i} \|dis(X, C_i)\|^2$$

where n signifies the dimension of the data object, and k is the number of clusters.

The k -means clustering algorithm computes the distance between each sample point and the cluster center. It starts by randomly selecting k sample objects from the dataset as the initial cluster centers. Through repeated iterations, it updates the position of each cluster center until either the updated cluster center remains unchanged or the change is below a certain threshold. Once the iterative algorithm concludes, the entire dataset is divided into k distinct clusters.

In this paper, to reduce the effect of outliers and missing values, a sliding average over a 365-day time span was used for NO₂ concentrations prior to the k -means analysis. Moreover, after several iterations using MATLAB (R2016a) software, we observed that the clustering results for some cities became unstable when the number of clusters exceeded 3, so this study classified the 100 cities into three categories for optimal stability.

2.3.2. Geographically and Temporally Weighted Regression Model (GTWR)

In contrast to the traditional ordinary least squares (OLS) model, the GWR model integrates spatial correlation and linear regression to enhance traditional models by examining the variable relationship’s spatial variability [37]. By conducting regional regression analysis on cross-sectional spatial data, GWR can detect spatial heterogeneity. However, it solely addresses the spatial nonstationarity of the sample data and disregards temporal nonstationarity. Huang et al. [31] developed the GTWR model by augmenting the GWR model with temporal coordinates, enabling a more comprehensive representation of spatial and temporal heterogeneity. The GTWR model can be expressed as follows:

$$Y_i = \beta_0(u_i, v_i, t_i) + \sum_k \beta_k(u_i, v_i, t_i) X_{ik} + \varepsilon_i$$

where Y_i is the dependent variable at the i th observation point, X_{ik} is the observed value of the k th independent variable at the i th observation point, (u_i, v_i, t_i) is the coordinate point (latitude, longitude, time) of the location of observation point i , $\beta_k(u_i, v_i, t_i)$ is the regression coefficient of the k th independent variable at the i th observation point, and ε_i is the error term.

The estimate for $\beta_k(u_i, v_i, t_i)$ can be expressed as follows:

$$\hat{\beta}_k(u_i, v_i, t_i) = [X^T W(u_i, v_i, t_i) X]^{-1} X^T W(u_i, v_i, t_i) Y$$

where, $W(u_i, v_i, t_i)$ equals $\text{diag}(w_{i1}, w_{i2}, \dots, w_{ij}, \dots, w_{in})$; w_{ij} denotes the space-time distance decay function of (u_i, v_i, t_i) , which corresponds to the weights used in the weighted regression of the calibration neighborhood observation i . In this work, employing spatiotemporal distances derived from Gaussian distance decay functions is as follows:

$$W_{ij} = \exp \left[-\frac{(d_{ij}^{ST})^2}{h^2} \right]$$

where h is a nonnegative quantity referred to as the bandwidth, which results in a decrease in impact as the distance increases. d_{ij}^{ST} denotes the measure of distance between point i and point j . which can be expressed as follows:

$$\left(d_{ij}^{ST}\right)^2 = \lambda[(u_i - u_j)^2 + (v_i - v_j)^2] + \mu(t_i - t_j)^2$$

where λ and μ are scaling factors that quantify the impact of distinct spatial and temporal distances within uncorrelated measurement systems, with neither λ nor μ being equal to zero.

The GTWR model requires at least one dependent variable and one or more independent variables, and the variance inflation factor (VIF) between these variables needs to be less than 10. In addition, the GTWR model requires the selection of an appropriate bandwidth, which determines the spatial extent over which neighboring data points influence the predictions at a given location. Selecting an optimal bandwidth is crucial to avoid underfitting or overfitting the data.

3. Results and Discussion

3.1. Classification of Urban NO₂ Concentration Level

Figure 2a shows a 365-day sliding average of hourly data from 100 cities. Figure 2b displays the curves representing the three types of cities: low NO₂ concentration cities (LNC), medium NO₂ concentration cities (MNC), and high NO₂ concentration cities (HNC), based on their respective NO₂ concentrations. The observed “U” change in NO₂ concentrations from late 2019 to the first half of 2020 can account for the outbreak of COVID-19 at the end of 2019. This significantly reduced NO₂ emissions from public transport and industrial sources during the first half of 2020. Consequently, the gradual resumption of production and work increased NO₂ concentrations [38].

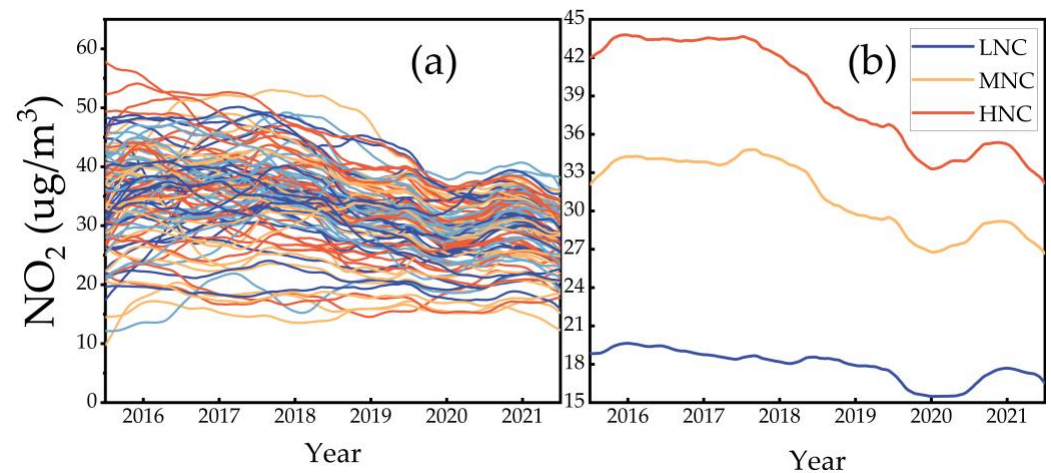


Figure 2. Sliding average (a) and *k*-means cluster analysis results (b). In (a), each line represents a different city.

The spatial distribution of the three city types is presented in Figure 3, comprising 15 cities in the LNC, 51 cities in the MNC, and 34 cities in the HNC. The LNC cities primarily consist of popular tourist locations such as Weihai and Huangshan, known for their robust tourism industries, picturesque landscapes, and good air quality. In contrast, the HNC encompasses major cities such as Shanghai, Nanjing, and Hefei alongside cities characterized by a robust industrial presence. The MNC category falls between the LNC and HNC categories.

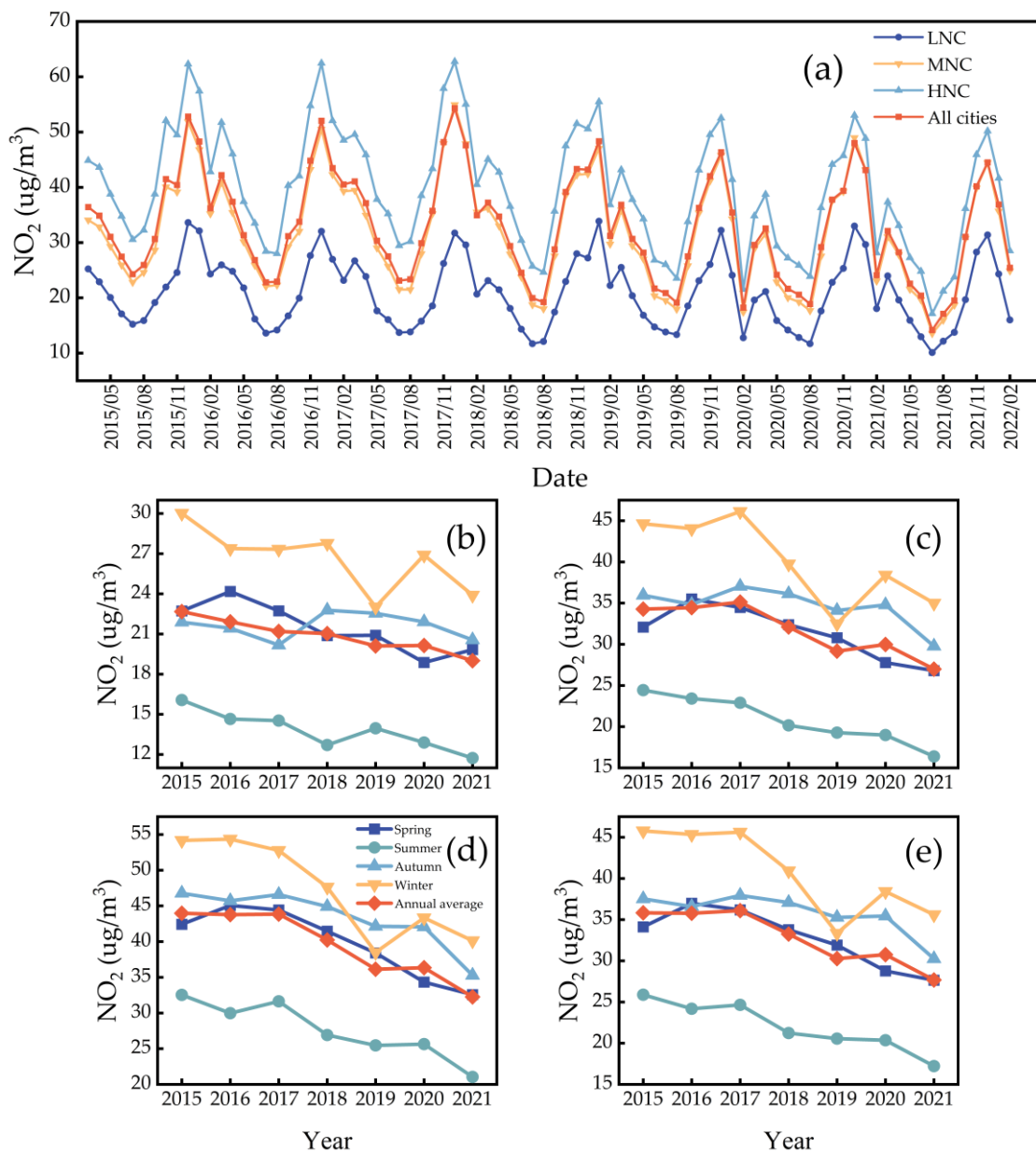


Figure 4. The monthly and seasonal distributions of NO₂ concentrations from 2015 to 2021. (a) Month changes in different types of cities; (b) LNC; (c) MNC; (d) HNC and (e) all city annual trends in NO₂ concentrations.

Figure 5 presents the percentage change in NO₂ concentrations from 2015 to 2021. Most cities observed a decrease in NO₂ concentrations exceeding 10%, and approximately 30% of places witnessed a decline of more than 30%. Bozhou City recorded the most substantial decline in NO₂ concentrations at 50.5%. However, a few cities exhibited an increase in NO₂ concentrations, with Luan City experiencing an increase of 29.5%. Bozhou, characterized by a well-established kiln industry, numerous enterprises employing boilers, and residents engaging in straw burning, has responded to national and local government policies by conducting an extensive optimization and environmentally conscious transformation of its kiln sector. The city has also enhanced the comprehensive utilization of straw among its population, resulting in a notable reduction in local NO_x concentrations. Conversely, Luan grapples with challenges pertaining to the management of pollutant emissions. Primarily originating from the iron and steel, glass, brick and tile, and building materials industries, the ongoing expansion of these sectors has gradually heightened NO_x emissions. This

underscores the persistent necessity for refining the industrial structure and transitioning to cleaner energy sources.

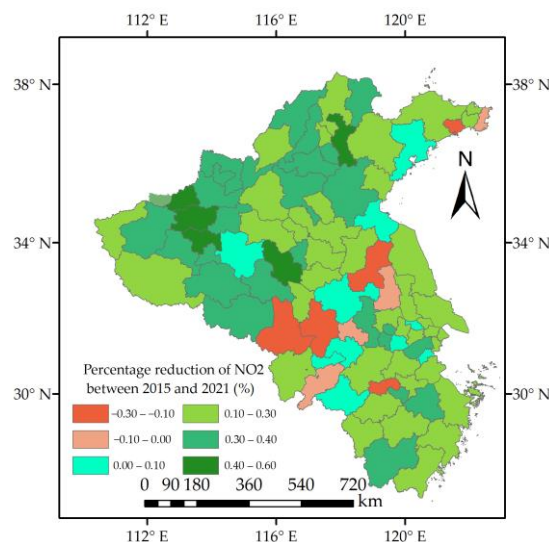


Figure 5. Percentage reduction in NO₂ concentration between 2015 and 2021.

3.3. Model Results

3.3.1. Model Parameter Results

Since the trends in NO₂ concentrations are the same for the three types of cities, the focus of this study is on their overall analysis using a model. Before model fitting, examining the covariance relationship among different variables is essential. Typically, a variance inflation factor (VIF) >10 indicates substantial multicollinearity between variables, which can significantly impact the model results. The test results are presented in Table 2. The VIF for the chosen economic components is all less than 10, suggesting the absence of significant multicollinearity among the variables, aligning with the requirements for GTWR model construction. When comparing the goodness of fit between the GWR and GTWR models, it becomes evident that the GTWR model exhibits a significantly higher R² than the GWR model. With the Akaike information criterion (AICC) serving as the model goodness-of-fit indicator, the GTWR model demonstrates a lower AICC value than the GWR model, and the residual sum of squares (RSS) for the GWR model exceeds that of the GTWR model, indicating superior goodness of fit for the GTWR model.

Table 2. Descriptive statistics of regression results of GWR and GTWR models.

		LNC	MNC	HNC	ALL	Meteorological	
Bandwidth	VIF	3.15–9.17	1.19–9.10	1.35–6.68	1.25–5.29	1.56–8.35	
	GWR	1.987	0.115	0.115	0.115	0.115	
RSS	GTWR	0.297	0.113	0.137	0.115	0.115	
	GWR	29.310	103.427	53.258	175.326	98.54	
AICC	GTWR	12.678	53.389	18.978	102.387	89.667	
	GWR	138.032	689.429	400.41	1062.62	943.56	
R ²	GTWR	137.187	614.578	365.268	947.706	824.84	
	GWR	0.402	0.638	0.707	0.662	0.795	
		GTWR	0.741	0.813	0.896	0.802	0.831

3.3.2. The Influence of Social Factors on Urban NO₂ Concentrations

Table 3 displays the distribution of coefficient estimates in the GTWR model, encompassing the minimum, lower quartile, median, upper quartile, and maximum values. Each indicator showcases a unique regression coefficient concerning the NO₂ concentration in each city. These coefficients exhibit substantial variability, emphasizing variations in influence degrees and associated trends. The positive and negative regression coefficients

reveal the dual effects of each indicator on urban NO₂, and the varying proportions of positive and negative impacts. This observation suggests spatial instability among the driving factors.

Table 3. Results for social factors in the GTWR model.

		Type of City	Min.	LQ	Med.	UQ	Max.
POP	Permanent population density	LNC	−2.339	−1.088	−0.573	−0.033	0.002
		MNC	−1.294	0.011	0.122	0.303	1.078
		HNC	−1.482	−0.328	−0.119	0.111	1.047
		ALL	−0.593	0.076	0.431	0.581	2.842
PGDP	GDP per capita	LNC	0.050	0.116	1.312	2.474	5.271
		MNC	−6.644	−0.938	−0.467	0.196	5.333
		HNC	−2.356	−1.076	−0.298	0.239	1.993
		ALL	−1.962	−0.645	−0.311	0.054	1.560
UR	Urbanization rate	LNC	−4.173	−2.292	−1.430	−0.502	−0.421
		MNC	−2.616	−0.356	0.181	0.592	6.396
		HNC	−2.054	−0.274	0.065	0.546	1.316
		ALL	−7.773	0.016	0.342	0.650	1.949
IS	Share of secondary sector output in total GDP	LNC	−0.705	−0.232	0.035	0.309	0.578
		MNC	−1.095	0.013	0.248	0.518	1.774
		HNC	−0.745	−0.108	0.158	0.399	1.331
		ALL	−0.151	0.252	0.393	0.516	1.436
EC	Electricity consumption of the whole society	LNC	−0.598	−0.158	0.241	0.688	0.781
		MNC	−1.934	−0.288	0.806	1.847	7.706
		HNC	−0.769	−0.197	0.147	0.457	2.118
		ALL	−1.148	0.168	0.520	0.840	2.508
CG	Coverage rate of urban green areas	LNC	−1.660	−0.798	−0.540	−0.198	−0.141
		MNC	−0.534	−0.062	0.101	0.228	1.366
		HNC	−0.754	−0.312	−0.073	0.104	0.409
		ALL	−0.433	−0.082	0.068	0.170	0.739
CV	Civil car vehicles	LNC	−0.402	−0.249	0.261	0.515	1.820
		MNC	−6.679	−2.100	−0.826	0.223	1.689
		HNC	−1.965	−0.240	0.201	0.657	1.970
		ALL	−1.634	−0.357	−0.036	0.210	1.299

The results of the GTWR indicate that the three types of cities have respective R² values of 0.741, 0.813, and 0.896, with an overall R² of 0.802. Furthermore, the coefficients of the GTWR model exhibit overall significance ($p < 0.05$). Additionally, the results of the GTWR model reveal varying impacts of socioeconomic factors on different types of cities. LNC demonstrates the highest positive correlation with PGDP (1.312) and the strongest negative correlation with the UR rate (−1.430). The highest correlation between EC (0.806) and CV (−0.826) is seen in MNC. Economic factors have a very constant impact on HNC, with PGDP (−0.298) and CV (0.201) having the most effects. These cities had the highest correlation with POP (0.431) and EC (0.520) overall.

Figure 6 represents the spatial distribution of average coefficients for various drivers in the GTWR model. The results indicate a positive correlation between population density and NO₂ concentration in most regions, particularly Shandong Province. Conversely, in some parts of Zhejiang Province, the correlation is negative. Moreover, the correlation between PGDP and NO₂ concentration exhibits significant regional variation. Specifically, regions in Zhejiang and Henan primarily display a negative correlation, while in Anhui and Shandong, the correlation is predominantly positive. The recent industrial expansion in Luan and Hefei has, to some extent, led to a significant depletion of resources and energy. This depletion could potentially be a contributing factor to the observed increase in NO₂ concentrations within these cities. Zhejiang exhibits the strongest positive correlation with the UR, while the IS positively correlates with NO₂ concentrations across all cities in the study area, particularly in Qingdao and Yantai in Shandong, suggesting that the secondary sector is one of the main sources of NO₂ emissions. The EC strongly affects urban NO₂ emissions in Henan while negatively affecting Anhui Province. The CG shows a negative correlation in certain parts of Henan and Zhejiang, whereas it demonstrates a positive correlation in most cities, particularly in Jiangsu Province. Regarding CV, Anhui Province exhibits a positive correlation, while Henan and Zhejiang primarily display a negative correlation. This finding aligns with the study by Carslaw et al. [40], which reports a decline in traffic-related NO₂ concentrations due to upgraded emission standards in

the automotive industry, predominantly attributed to reduced diesel vehicle emissions rather than light-duty vehicles. The 2022 Annual Report on Environmental Management of Mobile Sources in China (www.mee.gov.cn/hjzl/sthjzk/ydyhjgl/, accessed on 1 February 2023) confirms a similar trend.

Figure 7 illustrates the temporal distribution of average coefficients for various drivers in the GTWR model. Between 2015 and 2021, POP and CG were positively correlated with NO₂ concentrations, diminishing each year, and the negative correlation between PGDP and NO₂ concentrations increased. Although economic development can lead to environmental degradation, as income levels rise, environmental issues are expected to improve, leading to reduced pollutant emissions [41], which may be the main reason for the decrease in NO₂ concentration in Henan Province. The UR exhibits a “U” trend, implying that urbanization has been exacerbating environmental degradation in recent years [42]. The proportion of the IS and EC indicates an inverted “U” distribution. With the reinforcement of relevant laws and stringent regulations and the continuous adjustment of cleaning policies in recent years, China has been transitioning from a pollution-intensive secondary sector to a tertiary sector characterized by high value-added and advanced technology. This industrial and technological upgrade will help mitigate the negative impact on environmental quality [43].

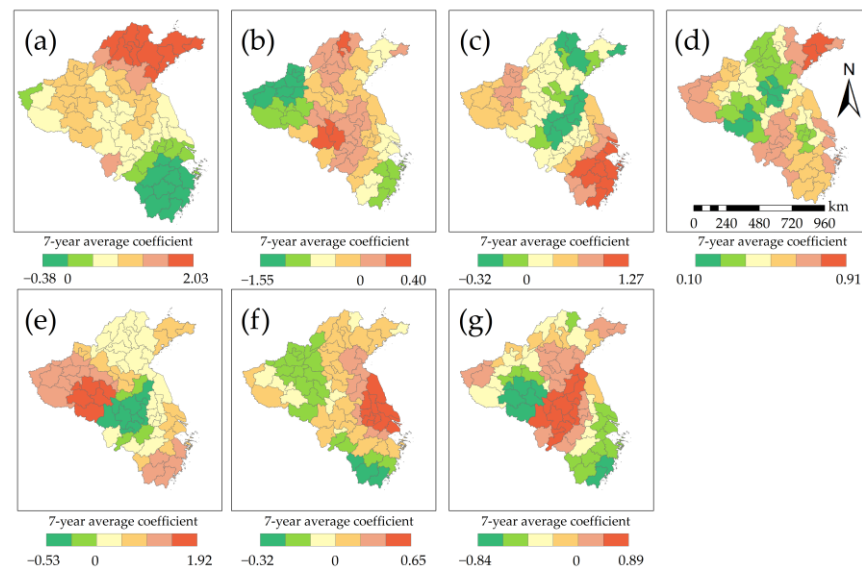


Figure 6. Spatial distribution of (a) POP, (b) PGDP, (c) UR, (d) IS, (e) EC, (f) CG, and (g) CV coefficients in the GTWR model.

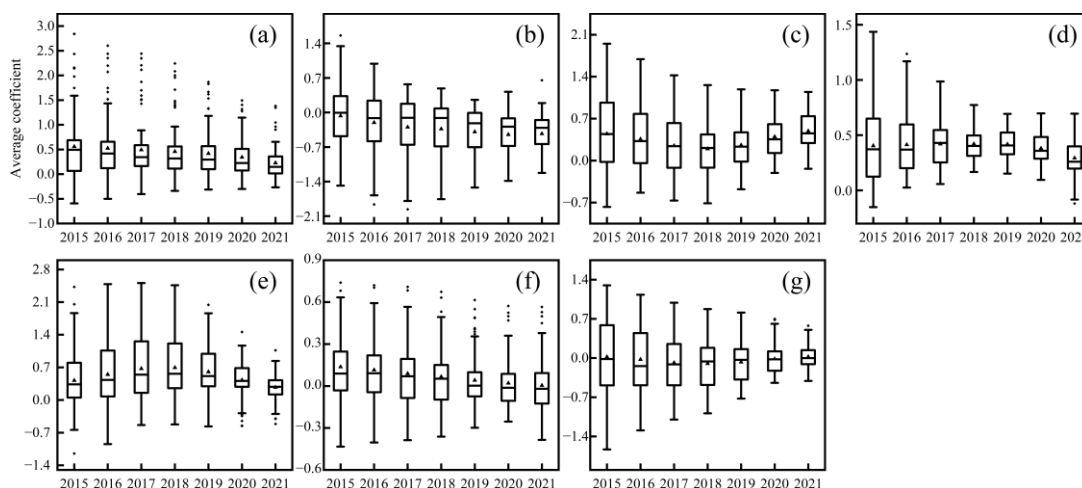


Figure 7. Temporal distribution of (a) POP, (b) PGDP, (c) UR, (d) IS, (e) EC, (f) CG, and (g) CV coefficients in the GTWR model.

3.3.3. The Influence of Meteorological Factors on Urban NO₂ Concentrations

Table 4 presents the results of global simulation coefficients for meteorological factors in the GTWR, and the coefficients of the GTWR model exhibit overall significance ($p < 0.05$). with an R^2 value of 0.831, suggesting a clear relationship between the variables and the variation in NO₂ concentration. The results indicate correlations between TEM, RHU, WIN, PRE, and NO₂ concentrations, with mean coefficients of -0.411 , -0.147 , -0.032 , and -0.116 , respectively. TEM exhibits a significant negative correlation with NO₂ concentration, displaying a correlation coefficient of -0.411 . The lower quartile (LQ) and upper quartile (UQ) values are -0.502 and -0.344 , respectively. As the temperature increases, the photochemical reaction rate of NO₂ intensifies [44].

Figure 8 illustrates the annual variations in the mean coefficients of various meteorological factors from 2015 to 2021. The average coefficients for TEM and RHU have generally decreased in recent years. The study found that the inhibitory effect of temperature on NO₂ concentration was most significant at lower temperatures and stabilized at higher temperatures. Additionally, NO₂ can be effectively removed from the air only when the relative humidity is high [45]. The trend of WIN is decreasing and then increasing; the average coefficient of PRE is increasing year by year, and the increase is most obvious in 2017.

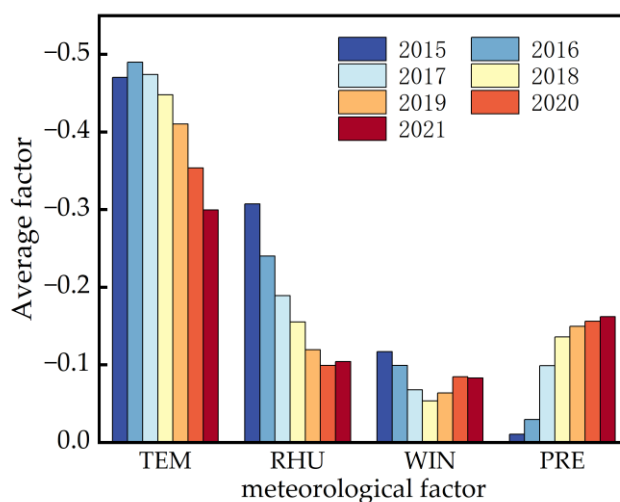


Figure 8. Annual variation in the mean coefficients of meteorological factors.

Table 4. Results for meteorological factors in the GTWR model.

	Min.	LQ	Med.	UQ	Max.
TEM	−0.951	−0.502	−0.411	−0.344	−0.064
RHU	−0.295	−0.251	−0.147	−0.022	0.479
WIN	−0.804	−0.417	−0.032	0.235	0.682
PRE	−0.588	−0.241	−0.116	−0.007	0.714

4. Conclusions

In this study, based on hourly NO₂ observations from 2015–2021, we classify cities in Mid-Eastern China into three categories by *k*-means clustering and explore the effects of drivers on spatial and temporal variations in NO₂ concentrations using the GTWR model. We concluded that the implementation of air pollution control policies in recent years has led to a reduction in NO₂ concentrations in most cities across mid-eastern China, although certain regions in Anhui and Jiangsu experienced exceptions to this trend. Furthermore, we observed a significant decrease in NO₂ levels during early 2020, attributed to the impact of COVID-19. Additionally, the seasonal variation in NO₂ concentration follows a distinct pattern, being higher in winter and lower in summer.

We carried out extensive data analysis in this paper and obtained some important conclusions. First, the strongest correlations of NO₂ concentration are found with POP and EC, which aligns with the consensus among researchers in this field [46,47]. This reaffirms the validity of our findings and underscores the reliability of our methodologies. Second, the relationships of NO₂ with socio-economic factors exhibit noticeable variations across different provinces, which contributes valuable insights into the visualization of spatial and temporal variations in the average coefficients of each of the related NO₂ concentrations, and future government policies should take into account the characteristics of different regions in formulating new development requirements. In conclusion, the study reveals the link between NO₂ concentrations and their possible influences, taking into account geographical differences and temporal dynamics. The empirical findings of this research highlight the unequivocal reality that air pollution challenges vary significantly across diverse Chinese cities. These disparities emerge due to pronounced spatial and temporal variations in the interplay between NO₂ concentrations and socioeconomic variables.

This study has the potential to inform government decision-making; however, it also reveals certain limitations that necessitate future research efforts. Primarily, the constraints associated with the NO₂ data obtained from meteorological stations hindered the classification of NO₂ emission sources, including transport, industry, and heating. Subsequent investigations should endeavor to incorporate more comprehensive and detailed data to facilitate more precise source analysis. Moreover, we selected and standardized seven social factors, which resulted in a smaller distribution of regression coefficients between the different factors. In addition, the complexity of the mechanisms of air pollution formation and comprehending urban NO₂ drivers through regression analysis remain challenges. Future research endeavors could employ a combined approach involving correlation analysis and chemical modeling to gain deeper insight into the multifaceted factors influencing NO₂ formation.

Author Contributions: Conceptualization, M.Y. and Y.J.; methodology, Y.J.; software, M.Y. and Y.J.; validation, M.Y., Y.J. and Q.Z.; formal analysis, M.Y. and Y.J.; investigation, Y.J. and Y.L.; data curation, Y.J., J.Q. and Y.L.; writing—original draft preparation, Y.J.; writing—review and editing, M.Y.; visualization, Y.J.; supervision, M.Y.; project administration, M.Y.; funding acquisition, M.Y. All authors have read and agreed to the published version of the manuscript.

Funding: This study was funded by the Research Foundation of Anhui Jianzhu University (2020QDZ31), the Anhui Provincial Key Laboratory of Environmental Pollution Control and Resource Reuse (2022EPC07), and the National Natural Science Foundation of China (41005016, 41105031).

Institutional Review Board Statement: Not applicable.

Informed Consent Statement: Not applicable.

Data Availability Statement: Hourly NO₂ observations were collected from the China National Environmental Monitoring Platform (<http://106.37.208.233:20035/>, accessed on 1 February 2023). Socioeconomic factor data were acquired from the National Statistical Database and the provincial and prefectural statistical yearbooks from 2015 to 2021. The meteorological data are from the National Centers for Environmental Information (<https://www.ncei.noaa.gov/>, accessed on 1 February 2023).

Acknowledgments: We want to express our sincere gratitude to the anonymous reviewers and editors for their efforts in improving the paper.

Conflicts of Interest: The authors declare no conflict of interest.

References

1. Zhang, L.; Wang, Y.; Feng, C.; Liang, S.; Liu, Y.; Du, H.; Jia, N. Understanding the industrial NO_x and SO₂ pollutant emissions in China from sector linkage perspective. *Sci. Total Environ.* **2021**, *770*, 145242. [[CrossRef](#)] [[PubMed](#)]
2. Fan, M.-Y.; Zhang, Y.-L.; Lin, Y.-C.; Li, L.; Xie, F.; Hu, J.; Mozaffar, A.; Cao, F. Source apportionments of atmospheric volatile organic compounds in Nanjing, China during high ozone pollution season. *Chemosphere* **2021**, *263*, 128025. [[CrossRef](#)] [[PubMed](#)]
3. Li, W.; Qi, Y.; Qu, W.; Qu, W.; Shi, J.; Zhang, D.; Liu, Y.; Zhang, Y.; Zhang, W.; Ren, D.; et al. PM_{2.5} source apportionment identified with total and soluble elements in positive matrix factorization. *Sci. Total Environ.* **2023**, *858*, 159948. [[CrossRef](#)] [[PubMed](#)]
4. Guan, W.-J.; Zheng, X.-Y.; Chung, K.F.; Zhong, N.-S. Impact of air pollution on the burden of chronic respiratory diseases in China: Time for urgent action. *Lancet* **2016**, *388*, 1939–1951. [[CrossRef](#)]
5. Xue, Y.; Wang, L.; Zhang, Y.; Zhao, Y.; Liu, Y. Air pollution: A culprit of lung cancer. *J. Hazard. Mater.* **2022**, *434*, 128937. [[CrossRef](#)] [[PubMed](#)]
6. Buoli, M.; Grassi, S.; Caldiroli, A.; Carnevali, G.S.; Mucci, F.; Iodice, S.; Cantone, L.; Pergoli, L.; Bollati, V. Is there a link between air pollution and mental disorders? *Environ. Int.* **2018**, *118*, 154–168. [[CrossRef](#)]
7. Deng, Q.; Lu, C.; Norbäck, D.; Bornehag, C.-G.; Zhang, Y.; Liu, W.; Yuan, H.; Sundell, J. Early life exposure to ambient air pollution and childhood asthma in China. *Environ. Res.* **2015**, *143*, 83–92. [[CrossRef](#)]
8. Itahashi, S.; Ge, B.; Sato, K.; Fu, J.S.; Wang, X.; Yamaji, K.; Nagashima, T.; Li, J.; Kajino, M.; Liao, H.; et al. MICS-Asia III: Overview of model intercomparison and evaluation of acid deposition over Asia. *Atmos. Chem. Phys.* **2020**, *20*, 2667–2693. [[CrossRef](#)]
9. Silvern, R.F.; Jacob, D.J.; Mickley, L.J.; Sulprizio, M.P.; Travis, K.R.; Marais, E.A.; Cohen, R.C.; Laughner, J.L.; Choi, S.; Joiner, J.; et al. Using satellite observations of tropospheric NO₂ columns to infer long-term trends in US NO_x emissions: The importance of accounting for the free tropospheric NO₂ background. *Atmos. Chem. Phys.* **2019**, *19*, 8863–8878. [[CrossRef](#)]
10. Huang, G.; Sun, K. Non-negligible impacts of clean air regulations on the reduction of tropospheric NO₂ over East China during the COVID-19 pandemic observed by OMI and TROPOMI. *Sci. Total Environ.* **2020**, *745*, 141023. [[CrossRef](#)]
11. Zheng, C.; Zhao, C.; Li, Y.; Wu, X.; Zhang, K.; Gao, J.; Qiao, Q.; Ren, Y.; Zhang, X.; Chai, F. Spatial and temporal distribution of NO₂ and SO₂ in Inner Mongolia urban agglomeration obtained from satellite remote sensing and ground observations. *Atmos. Environ.* **2018**, *188*, 50–59. [[CrossRef](#)]
12. De Hoogh, K.; Saucy, A.; Shtein, A.; Schwartz, J.; West, E.A.; Strassmann, A.; Puhon, M.; Rösli, M.; Stafoggia, M.; Kloog, I. Predicting Fine-Scale Daily NO₂ for 2005–2016 Incorporating OMI Satellite Data Across Switzerland. *Environ. Sci. Technol.* **2019**, *53*, 10279–10287. [[CrossRef](#)] [[PubMed](#)]
13. Bechle, M.J.; Millet, D.B.; Marshall, J.D. Remote sensing of exposure to NO₂: Satellite versus ground-based measurement in a large urban area. *Atmos. Environ.* **2013**, *69*, 345–353. [[CrossRef](#)]
14. Hůnová, I.; Baumelt, V.; Modlík, M. Long-term trends in nitrogen oxides at different types of monitoring stations in the Czech Republic. *Sci. Total Environ.* **2020**, *699*, 134378. [[CrossRef](#)]
15. Shen, Y.; Jiang, F.; Feng, S.; Xia, Z.; Zheng, Y.; Lyu, X.; Zhang, L.; Lou, C. Increased diurnal difference of NO₂ concentrations and its impact on recent ozone pollution in eastern China in summer. *Sci. Total Environ.* **2023**, *858*, 159767. [[CrossRef](#)]
16. Cui, Y.; Zha, H.; Dang, Y.; Qiu, L.; He, Q.; Jiang, L. Spatio-Temporal Heterogeneous Impacts of the Drivers of NO₂ Pollution in Chinese Cities: Based on Satellite Observation Data. *Remote Sens.* **2022**, *14*, 3487. [[CrossRef](#)]
17. Zheng, B.; Zhang, Q.; Geng, G.; Chen, C.; Shi, Q.; Cui, M.; Lei, Y.; He, K. Changes in China's anthropogenic emissions and air quality during the COVID-19 pandemic in 2020. *Earth Syst. Sci. Data* **2021**, *13*, 2895–2907. [[CrossRef](#)]
18. Li, R.; Wang, Z.; Cui, L.; Fu, H.; Zhang, L.; Kong, L.; Chen, W.; Chen, J. Air pollution characteristics in China during 2015–2016: Spatiotemporal variations and key meteorological factors. *Sci. Total Environ.* **2019**, *648*, 902–915. [[CrossRef](#)]
19. Yang, J.; Ji, Z.; Kang, S.; Zhang, Q.; Chen, X.; Lee, S.-Y. Spatiotemporal variations of air pollutants in western China and their relationship to meteorological factors and emission sources. *Environ. Pollut.* **2019**, *254*, 112952. [[CrossRef](#)]
20. Xu, B.; Zhong, R.; Liu, D.; Liu, Y. Investigating the impact of energy consumption and nitrogen fertilizer on NO_x emissions in China based on the environmental Kuznets curve. *Environ. Dev. Sustain.* **2021**, *23*, 17590–17605. [[CrossRef](#)]

21. Wang, J.; Ma, Y.; Qiu, Y.; Liu, L.; Dong, Z. Spatially differentiated effects of socioeconomic factors on China's NO_x generation from energy consumption: Implications for mitigation policy. *J. Environ. Manag.* **2019**, *250*, 109417. [[CrossRef](#)] [[PubMed](#)]
22. Wang, J.; Qiu, Y.; He, S.; Liu, N.; Xiao, C.; Liu, L. Investigating the driving forces of NO_x generation from energy consumption in China. *J. Clean. Prod.* **2018**, *184*, 836–846. [[CrossRef](#)]
23. Wang, J.; Li, X.; Ding, S.; Xu, X.; Liu, L.; Dong, L.; Feng, Y. Uncovering temporal-spatial drivers of vehicular NO_x emissions in China. *J. Clean. Prod.* **2021**, *288*, 125635. [[CrossRef](#)]
24. Xu, Y.; Zhang, W.; Huo, T.; Streets, D.G.; Wang, C. Investigating the spatio-temporal influences of urbanization and other socioeconomic factors on city-level industrial NO_x emissions: A case study in China. *Environ. Impact Assess. Rev.* **2023**, *99*, 106998. [[CrossRef](#)]
25. Zhang, G.; Han, J.; Su, B. Contributions of cleaner production and end-of-pipe treatment to NO_x emissions and intensity reductions in China, 1997–2018. *J. Environ. Manag.* **2023**, *326*, 116822. [[CrossRef](#)] [[PubMed](#)]
26. He, S.; Zhao, L.; Ding, S.; Liang, S.; Dong, L.; Wang, J.; Feng, Y.; Liu, L. Mapping economic drivers of China's NO_x emissions due to energy consumption. *J. Clean. Prod.* **2019**, *241*, 118130. [[CrossRef](#)]
27. Enkhbat, E.; Geng, Y.; Zhang, X.; Jiang, H.; Liu, J.; Wu, D. Driving Forces of Air Pollution in Ulaanbaatar City Between 2005 and 2015: An Index Decomposition Analysis. *Sustainability* **2020**, *12*, 3185. [[CrossRef](#)]
28. Guo, S.; Liu, G.; Liu, S. Driving factors of NO_x emission reduction in China's power industry: Based on LMDI decomposition model. *Environ. Sci. Pollut. Res.* **2023**, *30*, 51042–51060. [[CrossRef](#)]
29. Liu, X.; Yi, G.; Zhou, X.; Zhang, T.; Lan, Y.; Yu, D.; Wen, B.; Hu, J. Atmospheric NO₂ Distribution Characteristics and Influencing Factors in Yangtze River Economic Belt: Analysis of the NO₂ Product of TROPOMI/Sentinel-5P. *Atmosphere* **2021**, *12*, 1142. [[CrossRef](#)]
30. Yang, L.; Qin, C.; Li, K.; Deng, C.; Liu, Y. Quantifying the Spatiotemporal Heterogeneity of PM_{2.5} Pollution and Its Determinants in 273 Cities in China. *IJERPH* **2023**, *20*, 1183. [[CrossRef](#)]
31. Huang, B.; Wu, B.; Barry, M. Geographically and temporally weighted regression for modeling spatio-temporal variation in house prices. *Int. J. Geogr. Inf. Sci.* **2010**, *24*, 383–401. [[CrossRef](#)]
32. Chen, Y.; Chen, M.; Huang, B.; Wu, C.; Shi, W. Modeling the Spatiotemporal Association Between COVID-19 Transmission and Population Mobility Using Geographically and Temporally Weighted Regression. *GeoHealth* **2021**, *5*, e2021GH000402. [[CrossRef](#)] [[PubMed](#)]
33. Zhao, M.; Wang, H.; Sun, J.; Tang, R.; Cai, B.; Song, X.; Huang, X.; Huang, J.; Fan, Z. Spatio-temporal characteristics of soil Cd pollution and its influencing factors: A Geographically and temporally weighted regression (GTWR) method. *J. Hazard. Mater.* **2023**, *446*, 130613. [[CrossRef](#)]
34. Zhang, W.; Wang, J.; Xu, Y.; Wang, C.; Streets, D.G. Analyzing the spatio-temporal variation of the CO₂ emissions from district heating systems with “Coal-to-Gas” transition: Evidence from GTWR model and satellite data in China. *Sci. Total Environ.* **2022**, *803*, 150083. [[CrossRef](#)]
35. GB 3095-2012; Ambient Air Quality Standards. Ministry of Environmental Protection of PRC: Beijing, China, 2012.
36. Ikotun, A.M.; Ezugwu, A.E.; Abualigah, L.; Abuhaija, B.; Heming, J. K-means clustering algorithms: A comprehensive review, variants analysis, and advances in the era of big data. *Inf. Sci.* **2023**, *622*, 178–210. [[CrossRef](#)]
37. Brunson, C.; Fotheringham, A.S.; Charlton, M.E. Geographically Weighted Regression: A Method for Exploring Spatial Nonstationarity. *Geogr. Anal.* **1996**, *28*, 281–298. [[CrossRef](#)]
38. Wang, Z.; Uno, I.; Yumimoto, K.; Itahashi, S.; Chen, X.; Yang, W.; Wang, Z. Impacts of COVID-19 lockdown, Spring Festival and meteorology on the NO₂ variations in early 2020 over China based on in-situ observations, satellite retrievals and model simulations. *Atmos. Environ.* **2021**, *244*, 117972. [[CrossRef](#)]
39. Li, D.; Wu, Q.; Wang, H.; Xiao, H.; Xu, Q.; Wang, L.; Feng, J.; Yang, X.; Cheng, H.; Wang, L.; et al. The Spring Festival Effect: The change in NO₂ column concentration in China caused by the migration of human activities. *Atmos. Pollut. Res.* **2021**, *12*, 101232. [[CrossRef](#)]
40. Carslaw, D.C.; Murrells, T.P.; Andersson, J.; Keenan, M. Have vehicle emissions of primary NO₂ peaked? *Faraday Discuss.* **2016**, *189*, 439–454. [[CrossRef](#)]
41. Ding, Y.; Zhang, M.; Chen, S.; Wang, W.; Nie, R. The environmental Kuznets curve for PM_{2.5} pollution in Beijing-Tianjin-Hebei region of China: A spatial panel data approach. *J. Clean. Prod.* **2019**, *220*, 984–994. [[CrossRef](#)]
42. Zhu, Y.; Zhan, Y.; Wang, B.; Li, Z.; Qin, Y.; Zhang, K. Spatiotemporally mapping of the relationship between NO₂ pollution and urbanization for a megacity in Southwest China during 2005–2016. *Chemosphere* **2019**, *220*, 155–162. [[CrossRef](#)] [[PubMed](#)]
43. Liu, F.; Zhang, Q.; van der A, R.; Zheng, B.; Tong, D.; Yan, L.; Zheng, Y.; He, K. Recent reduction in NO_x emissions over China: Synthesis of satellite observations and emission inventories. *Environ. Res. Lett.* **2016**, *11*, 114002. [[CrossRef](#)]
44. Wang, C.; Wang, T.; Wang, P. The Spatial–Temporal Variation of Tropospheric NO₂ over China during 2005 to 2018. *Atmosphere* **2019**, *10*, 444. [[CrossRef](#)]
45. Ju, T.; Geng, T.; Li, B.; An, B.; Huang, R.; Fan, J.; Liang, Z.; Duan, J. Impacts of Certain Meteorological Factors on Atmospheric NO₂ Concentrations during COVID-19 Lockdown in 2020 in Wuhan, China. *Sustainability* **2022**, *14*, 16720. [[CrossRef](#)]

46. Zhan, D.; Kwan, M.-P.; Zhang, W.; Wang, S.; Yu, J. Spatiotemporal Variations and Driving Factors of Air Pollution in China. *IJERPH* **2017**, *14*, 1538. [[CrossRef](#)]
47. Wang, L.; Wang, Y.; He, H.; Lu, Y.; Zhou, Z. Driving force analysis of the nitrogen oxides intensity related to electricity sector in China based on the LMDI method. *J. Clean. Prod.* **2020**, *242*, 118364. [[CrossRef](#)]

Disclaimer/Publisher's Note: The statements, opinions and data contained in all publications are solely those of the individual author(s) and contributor(s) and not of MDPI and/or the editor(s). MDPI and/or the editor(s) disclaim responsibility for any injury to people or property resulting from any ideas, methods, instructions or products referred to in the content.